International Journal of Electrical, Electronic and Communication Sciences
ISSN: 2517-9438
Vol:9, No:1, 2015

Analysis of Nonlinear Pulse Propagation Characteristics in Semiconductor Optical Amplifier for Different Input Pulse Shapes

Suchi Barua, Narottam Das, Sven Nordholm, Mohammad Razaghi

***Abstract*—**This paper presents nonlinear pulse propagation characteristics for different input optical pulse shapes with various input pulse energy levels in semiconductor optical amplifiers. For simulation of nonlinear pulse propagation, finite-difference beam propagation method is used to solve the nonlinear Schrödinger equation. In this equation, gain spectrum dynamics, gain saturation are taken into account which depends on carrier depletion, carrier heating, spectral-hole burning, group velocity dispersion, self-phase modulation and two photon absorption. From this analysis, we obtained the output waveforms and spectra for different input pulse shapes as well as for different input energies. It shows clearly that the peak position of the output waveforms are shifted toward the leading edge which due to the gain saturation of the SOA for higher input pulse energies. We also analyzed and compared the normalized difference of full-width at half maximum for different input pulse shapes in the SOA.

***Keywords*—**Finite-difference beam propagation method, pulse shape, pulse propagation, semiconductor optical amplifier.

I. Introduction

NOWADAYS, in high-speed communication systems, all-optical signal processing techniques play an important role to avoid electro-optic conversions which may create data-flow bottlenecks. Semiconductor optical amplifiers (SOAs) are widely used in many functional applications, such as wavelength conversion, optical switching, optical signal processing pulse reshaping, and power limiting [1], [2]. SOAs are the key component for optical amplification and optical switching at a very high speed because of their small size, a low switching energy, non-linear characteristics and ability to integrate with other optical devices [3].

Active SOAs are essential components in many recently proposed systems for high-speed optical communications and signal processing. Hence, a detail characterization and theoretical modeling of the short-pulses gain saturation is important in order to understand the fundamental limitations of these devices and improve their performances in optical communication and signal processing. The purpose of modelling an SOA is to relate the internal variables of the amplifier with external characteristics, such as output signal power, output saturation power [3]. The modified nonlinear Schrödinger equation (MNLSE) is commonly used in most pulse propagation models that included the SOA non-linearities [4]. The pulse propagation through an SOA is strongly dependent on the SOA input pulse shapes [5].

The main objective of this paper is to investigate the nonlinear optical pulse propagation for different types of input pulse shapes with different input energy levels in the SOAs for high speed communication systems. This analysis is based on the MNLSE considering the self-phase modulation (SPM), two-photon absorption (TPA), group velocity dispersion (GVD), carrier depletion (CD), carrier heating (CH), spectral-hole burning (SHB), gain spectrum dynamics, and gain saturation in the SOA [6]-[11]. To solve the MNLSE, finite-difference beam propagation method (FD-BPM) is used because of its short convergence time and excellent accuracy of the simulated results [6], [7]. For simulation of nonlinear pulse propagation with small propagation steps, FD-BPM is considered as the best method comparing other methods [7]-[11].

In this paper, we analyzed and compared the single pulse propagation characteristics. We also investigated the normalized difference of full width at half maximum (FWHM) after propagation of pulses for different types of input pulse shapes. This paper is organized as follows. Section II describes the theoretical model of nonlinear pulse propagation in SOAs. The simulation results and discussion are presented in section III. Finally, the conclusion is in Section IV.

II. Theoretical Model of SOAs

The following MNLSE is used for the simulation of nonlinear pulse propagation in SOAs with different input pulse shapes [4], [6]-[11].

$$\left[\frac{\partial}{\partial z}-\frac{i}{2}\beta_2\frac{\partial^2}{\partial\tau^2}+\frac{\gamma}{2}+\left(\frac{\gamma_{2p}}{2}+ib_2\right)\left|V(\tau,z)\right|^2\right]V(\tau,z)$$
$$=\left\{\frac{1}{2}g_N(\tau)\left[\frac{1}{f(\tau)}+i\alpha_N\right]+\frac{1}{2}\Delta g_T(\tau)(1+i\alpha_T)\right.$$
$$\left.-i\frac{1}{2}\frac{\partial g(\tau,\omega)}{\partial\omega}|_{\omega_0}\frac{\partial}{\partial\tau}-\frac{1}{4}\frac{\partial^2 g(\tau,\omega)}{\partial\omega^2}|_{\omega_0}\frac{\partial^2}{\partial\tau^2}\right\}V(\tau,z) \quad (1)$$

Suchi Barua and Sven Nordholm are with the Department of Electrical and Computer Engineering, Curtin University, Perth, Australia (e-mail: suchi.barua@student.curtin.edu.au, s.nordholm@curtin.edu.au)

Narottam Das is with the School of Mechanical and Electrical Engineering, The University of Southern Queensland, Toowoomba, Queensland, Australia (e-mail: Narottam.Das@usq.edu.au), Department of Electrical and Computer Engineering, Curtin University Sarawak, Miri, Malaysia (e-mail: narottam@curtin.edu.my).

Mohammad Razaghi is with the Department of Electrical and Computer Engineering, University of Kurdistan, Iran (email: m.razaghi@uok.ac.ir).

where,

$$g_N(\tau) = g_0 \exp\left(-\frac{1}{W_s} \int_{-\infty}^{\tau} e^{-s/\tau_s} \left|V(s)\right|^2 ds \right) \quad (2)$$

$$f(\tau) = 1 + \frac{1}{\tau_{shb} P_{shb}} \int_{-\infty}^{+\infty} u(s) e^{-s/\tau_{shb}} \left|V(\tau - s)\right|^2 ds \quad (3)$$

$$\Delta g_T(\tau) = -h_1 \int_{-\infty}^{+\infty} u(s) e^{-s/\tau_{ch}} (1 - e^{-s/\tau_{shb}}) \left|V(\tau - s)\right|^2 ds$$
$$-h_2 \int_{-\infty}^{+\infty} u(s) e^{-s/\tau_{ch}} (1 - e^{-s/\tau_{shb}}) \left|V(\tau - s)\right|^4 ds \quad (4)$$

$$\left.\frac{\partial g(\tau,\omega)}{\partial \omega}\right|_{\omega_0} = A_1 + B_1\left[g_0 - g(\tau,\omega_0)\right] \quad (5)$$

$$\left.\frac{\partial^2 g(\tau,\omega)}{\partial \omega^2}\right|_{\omega_0} = A_2 + B_2\left[g_0 - g(\tau,\omega_0)\right] \quad (6)$$

$$g(\tau,\omega_0) = g_N(\tau,\omega_0) / f(\tau) + \Delta g_T(\tau,\omega_0) \quad (7)$$

Here, we introduce the frame of the local time $\tau\ (= t - z/v_g)$ which propagates with the group velocity v_g at the centre frequency of an optical pulse. The slowly varying envelope approximation is used in (1), where the temporal variation change of the complex envelope function is very slow compared with the cycle of an optical field. In (1), $V(\tau, z)$ is the time domain complex envelope function of an optical pulse, $|V(\tau,z)|^2$ corresponds to the optical power, and β_2 is the GVD. γ is the linear loss, γ_{2p} is the TPA coefficient, $b_2 (= \omega_0 n_2 / cA)$ is the instantaneous SPM term due to the instantaneous nonlinear refractive index n_2 (Kerr effect), $\omega_0 (= 2\pi f_0)$ is the centre angular frequency of the pulse, c is the velocity of light in vacuum, $A (= wd/\Gamma)$ is the effective area (d and w are the thickness and width of the active region, respectively, and Γ is the confinement factor). $g_N(\tau)$ is the saturated gain due to CD g_0 is the linear gain, W_s is the saturation energy, τ_s is the carrier lifetime, $f_{(\tau)}$ is the SHB function, P_{shb} is the SHB saturation power, τ_{shb} is the SHB relaxation time, and α_N and α_T the line width enhancement factor associated with the gain changes due to the CD and CH. $\Delta g_T(\tau)$ is the resulting gain change due to the CH and TPA $u(s)$ is the unit step function, τ_{ch} the CH relaxation time, h_1 is the contribution of stimulated emission and free-carrier absorption to the CH gain reduction, and h_2 is the contribution of TPA. Finally, A_1 and A_2 are the slope and the curvature of the linear gain at ω_0 respectively, while B_1 and B_2 are constants describing changes in these quantities with saturation. In this simulation, the gain spectrum of an SOA is approximated by the following second-order Taylor expansion in $\Delta\omega$:

$$g(\tau,\omega) = g(\tau,\omega_0) + \Delta\omega \left.\frac{\partial g(\tau,\omega)}{\partial \omega}\right|_{\omega_0} + \frac{(\Delta\omega)^2}{2} \left.\frac{\partial^2 g(\tau,\omega)}{\partial \omega^2}\right|_{\omega_0} \quad (8)$$

The coefficients $\partial g(\tau,\omega)/\partial\omega\big|_{\omega_0}$ and $\partial^2 g(\tau,\omega)/\partial\omega^2\big|_{\omega_0}$ are related to A_1, A_2, B_1 and B_2 as given by (5) and (6). We assumed the same values of A_1, A_2, B_1 and B_2 as for an AlGaAs/GaAs bulk SOA.

Generally, the fast Fourier transformation BPM (FFT-BPM) is used for analysis of the optical pulse propagation in optical fibers by successive iterations of the Fourier transformation and the inverse Fourier transformation. In the FFT-BPM, the linear propagation term (GVD term) and phase compensation terms (other than GVD, first- and second- order gain spectrum terms) will be separated in the nonlinear Schrödinger equation for the individual consideration of the time and frequency domain for the optical pulse propagation. However, in our model, (1) includes the dynamic gain change terms, i.e., the first- and second- order gain spectrum terms which are the last two terms of the right side in (1). Therefore, it is not possible to separate (1) into the linear propagation term and phase compensation term, and it is difficult to calculate (1) using the FFT-BPM. For this reason, we have used the FD-BPM to solve this MNLSE [7]-[11].

III. Simulation Results and Discussion

In this section, simulation results of single nonlinear optical pulse propagation and normalized difference of FWHM are discussed for different input pulse shapes. For the simulation, the parameters of a bulk SOA (AlGaAs/GaAs, double heterostructure) is used. The parameters are listed in Table I [7], [9].

TABLE I
List of the Parameters Used in Simulation [7], [9]

Parameters	Symbols	Values	Units
Length of SOA	L	500	μm
Effective area	A	5	μm^2
Centre frequency of the pulse	f_0	349	THz
Linear gain	g_0	92	cm^{-1}
Group velocity dispersion	β_2	0.05	$ps^2 cm^{-1}$
Saturation energy	W_s	80	pJ
Linewidth enhancement factor due to the carrier depletion	α_N	3.1	
Linewidth enhancement factor due to the carrier heating	α_T	2.0	
The contribution of stimulated emission and free carrier absorption to the carrier heating gain reduction	h_1	0.13	$cm^{-1} pJ^{-1}$
The contribution of two-photon absorption	h_2	126	$fscm^{-1} pJ^{-2}$
Carrier lifetime	τ_s	200	Ps
Carrier heating relaxation time	τ_{ch}	700	Fs
Spectral-hole burning relaxation time	τ_{shb}	60	Fs
Spectral-hole burning saturation power	P_{shb}	28.3	W
Linear loss	γ	11.5	cm^{-1}
Instantaneous nonlinear Kerr effect	n_2	-0.70	$cm^2 TW^{-1}$
Two-photon absorption coefficient	γ_{2p}	1.1	$cm^{-1}W^{-1}$
Parameter describing second-order Taylor expansion of the dynamically gain spectrum.	A_1	0.15	$fs\ \mu m^{-1}$
	B_1	-80	fs
	A_2	-60	$fs^2\ \mu m^{-1}$
	B_2	0	fs^2

A. Nonlinear Optical Pulse Propagation Characteristics

For the simulation of nonlinear pulse propagation in SOA, the length of the SOA is considered 500μm and we have

obtained all the results with a propagation step Δz of 10μm. Different types of input pulse shapes are considered, such as (i) Secant hyperbolic pulse, (ii) Gaussian pulse, and (iii) Lorentzian-shaped pulse.

Fig. 1 illustrates a simulation model for the propagation of nonlinear optical pulses in an SOA. An optical pulse is injected into the input facet of the SOA, where the input pulse position is at $z = 0$. The pulse propagated over the length 500-μm of the SOA. Here, τ is the local time, $|V(\tau,0)|^2$ is the intensity (power) of input pulse ($z = 0$) and $|V(\tau,z)|^2$ is the intensity (power) of the output pulse after propagating a distance z (=500-μm) at the output side of SOA [11].

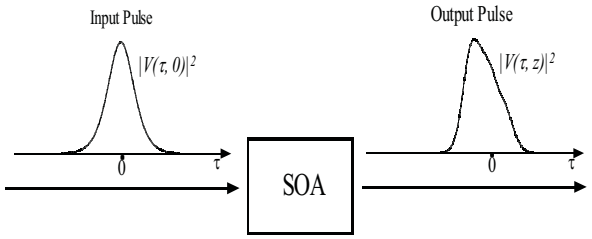

Fig. 1 Schematic diagram for the simulation of nonlinear propagation pulses in SOA. Here, $|V(\tau, 0)|^2$ and $|V(\tau, z)|^2$ are the input and output (after propagating a distance z) pulses of the SOA

Fig. 2 shows the simulation results of nonlinear optical pulse propagation characteristics in an SOA, when the input pulse width is 10 ps. The output waveforms for Secant hyperbolic pulse shape, Gaussian pulse shape and Lorentzian pulse shape are shown in Fig. 2 (i) when the input pulse energies are (a) 2 pJ, (b) 1 pJ and (c) 500 fJ, respectively. The sampling time step (Δt) is considered as 0.025 ps. It is clearly observed that higher output pulse energy is achieved by Gaussian pulse and lower output energy is achieved by Lorentzian pulse for all the level of input pulse energies (high to low). The calculated peak output powers are 4.2693 W, 4.5268 W, and 4.0091 W for Secant hyperbolic, Gaussian and Lorentzian pulses, respectively when input energy is 2 pJ. For the input energy 1 pJ, the calculated peak output powers are 2.89 W, 3.06 W and 2.71 W for Secant hyperbolic, Gaussian and Lorentzian pulses, respectively. However, when the input energy is low (i.e., 500 fJ), the calculated peak output powers are 1.77 W, 1.88 W, and 1.66 W for Secant hyperbolic, Gaussian and Lorentzian pulses, respectively. From these results, it can be confirmed that the higher output pulse energy can be achieved for higher input energy for all those three pulse shapes and vice versa. As the input pulse width is very shorter than the considered carrier lifetime, the leading edge of the pulse saturates the amplifier and the trailing edge experiences a lower gain, so the output pulse shape becomes asymmetric. Comparing all three pulse shapes with different input pulse energy levels, it can be observed that the output pulse shapes become more asymmetric for higher input energy and less asymmetric for the lower input energy levels.

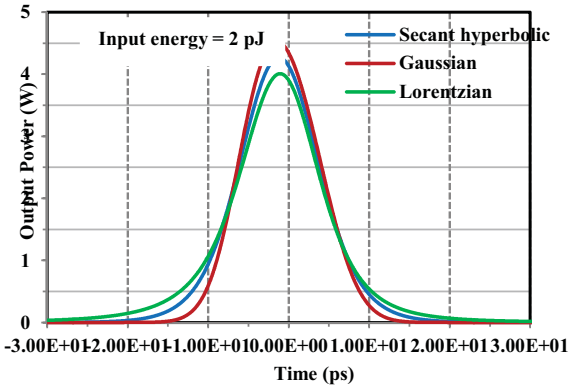

(a)

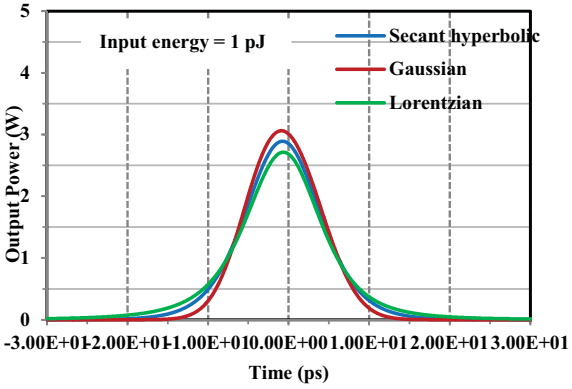

(b)

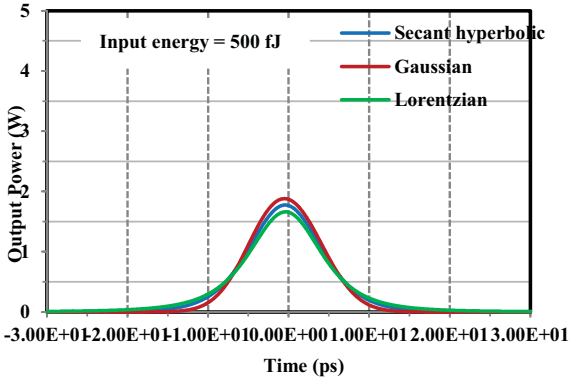

(c)

Fig. 2 (i) Output waveform for Secant hyperbolic pulse, Gaussian pulse and Lorentzian pulse when input energies are: (a) 2 pJ, (b) 1 pJ and (c) 500 fJ

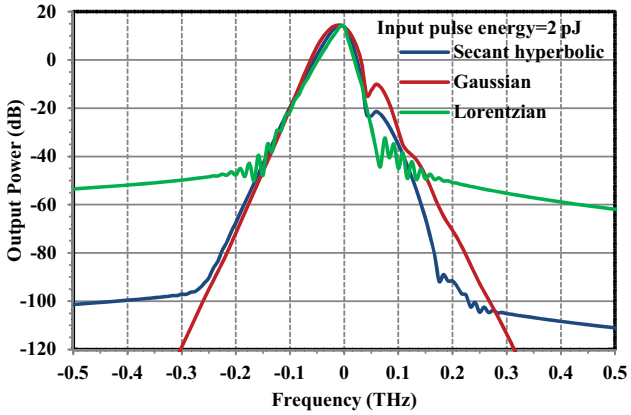

(a)

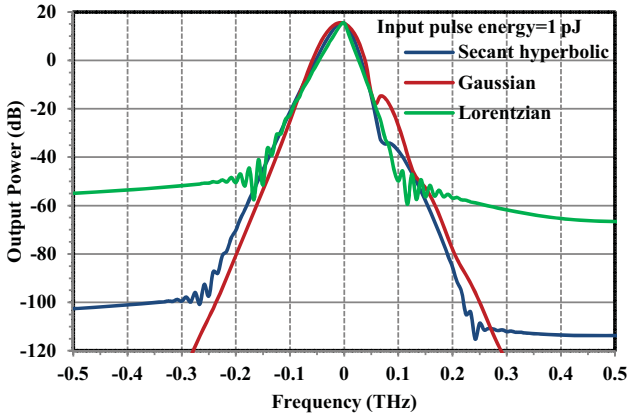

(b)

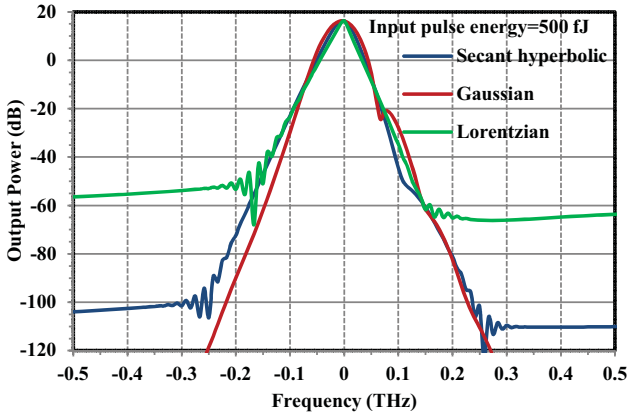

(c)

Fig. 2 (ii) Output spectra for Secant hyperbolic pulse, Gaussian pulse and Lorentzian pulses when input energies are: (a) 2 pJ, (b) 1 pJ and (c) 500 fJ

Fig. 2 (ii) shows the frequency spectra of propagated output pulses for Secant hyperbolic pulse shape, Gaussian pulse shape and Lorentzian pulse shapes when the input pulse energies are: (a) 2 pJ, (b) 1 pJ, and (c) 500 fJ. The frequency spectra were obtained by performing the FFT on the temporal pulse shapes as shown in Fig. 2 (i). The output spectral shape shifting is observed toward the lower frequency side, which is due to the gain saturation of the SOA and the SPM effects. For weak input pulse energies (i.e., ≤500 fJ), none of the output frequency spectra has been shifted toward the lower frequency side. It can be clearly seen from these figures that the output spectra is red-shifted and the amount of frequency shift is ~ -8.3 GHz for Secant hyperbolic and Gaussian pulses when the input pulse energy is 2 pJ and 1 pJ. While there is no red shifting is occurring for the Lorentzian pulse when the input pulse energy is 2pJ and 1 pJ. A wider spectral broadening is observed for Gaussian pulse compared to the other pulses, when the input energy is 2 pJ. Besides that some oscillatory structures (i.e., dips) are observed in the upper frequency side of the frequency spectra, which is due to the SPM effects [7], [8]. The physical mechanism behind the spectral shift and distortion is the SPM, occurring as a result of index nonlinearities induced by the gain saturation [7]-[9]. From the simulated results, it has confirmed that there is no red shifting occurs in Lorentzian pulses for the considered pulse energies (i.e., 500 fJ ~ 2 pJ).

A. Normalized Difference of FWHM

Fig. 3 shows the normalized difference of FWHM versus input FWHM for different input pulse energies for (a) Secant hyperbolic pulse, (b) Gaussian pulse and (c) Lorentzian pulse. To achieve the results, autocorrelation trace is used to analyze the series of data with normalization waveforms. We have investigated how the output FWHM varies with the input FWHM and input pulse energies for different input pulse shapes. For particular input pulse energy, a higher percentage of increased output FWHM can be found for lower input FWHM and vice versa. For example, when the input pulse energy is 2 pJ, the output FWHM increases by 15.2%, 19.29%, 24.4%, 35% and 62.5% for the input FWHM of 10 ps, 7 ps, 5 ps, 3 ps and 1 ps, for the Secant hyperbolic pulse.

The similar results have been obtained for all three considered pulse shapes in this case study. It has been also observed that with the decrease of input pulse energy the percentage of increased output FWHM decreases for all input FWHM. From above observation, it can be concluded that, for a higher input energy with lower in put FWHM, the variation of output FWHM is the highest and lowest variation in output FWHM can be found for lower input energy with higher FWHM. Also in this case study, similar results have been calculated for all those three input pulses. But highest percentage of increased output FWHM has been calculated for Lorentzian pulse for all considered input energy along with input FWHM. For example, variation of output FWHM increases by 16%, 15.2% and 12.5% for Lorentzian pulse, Secant hyperbolic and Gaussian pulse respectively, when input pulse energy is 2 pJ and the input FWHM is 10 ps.

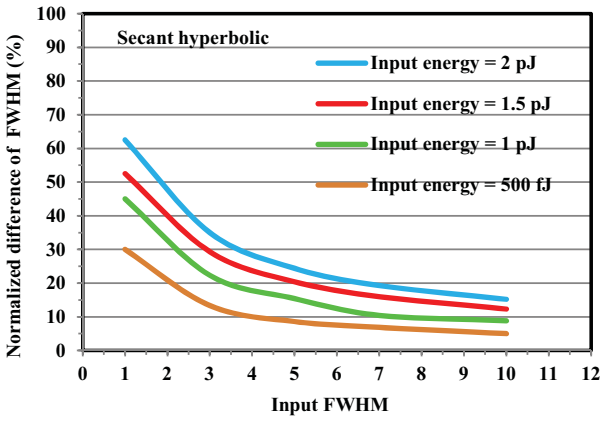

(a)

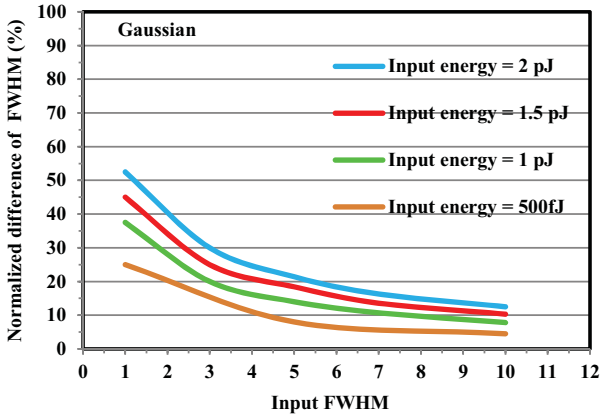

(b)

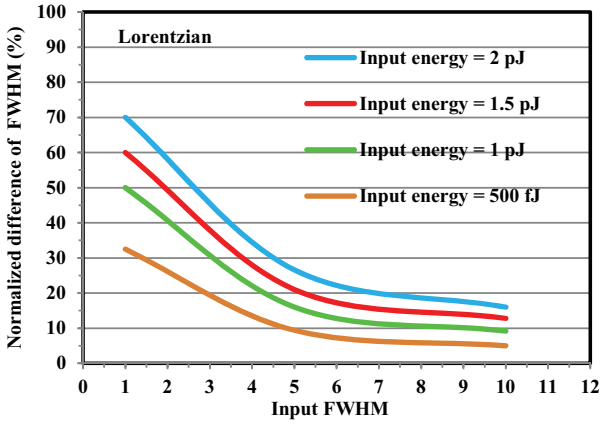

(c)

Fig. 3 Normalized difference of FWHM versus input FWHM for different input pulse energy levels for (a) Secant hyperbolic pulse, (b) Gaussian pulse, and (c) Lorentzian pulse

IV. Conclusion

In this paper, nonlinear optical pulse propagation characteristics have been analyzed for different input pulse shapes with different input pulse energy levels in SOAs. The higher output pulse energy is achieved for Gaussian pulse shape and the lower output pulse energy is achieved for Lorentzian pulse shape for all the considered input pulse energy levels. From the output frequency spectra, it has clearly observed that red shifting does not occur for Lorentzian pulse for the considered input pulse energies (i.e., 500 fJ ~ 2 pJ). The difference between the output and input FWHM of pulses also has been calculated for different input pulse shapes with the increase of input FWHM after normalizing the output pulse power. From the simulated results, it can be concluded that the percentage of FWHM increases with the decrease of input FWHM and decreases with the increase of input FWHM. The simulation results are useful for next generation high-speed optical network/ communication systems as the device has nonlinearities.

References

[1] P. P. Baveja, A. M. Kaplan, D. N. Maywar, G. P. Agrawal, "Pulse amplification in semiconductor optical amplifiers with ultrafast gain-recovery times" in proc. of SPIE 7598, Optical Components and Materials VII, vol. 7598, pp. 2-11, February, 2010.

[2] A. A. E. Aziz, W. P. Ng, Z. Ghassemlooy, M. H. Aly, and M. F. Chiang, "Optimisation of the key SOA parameters for amplification and switching" in proc. of the 9th Annual Postgraduate Symposium on the Convergence of Telecommunications, Networking & Broadcasting, PGNET, Liverpool, pp. 107-111, 2008.

[3] A. A. Shalaby, "Characterisation and optimisation of the semiconductor optical amplifier for ultra-high speed performance", Doctoral Dissertation, Northumbria University, Newcastle, UK, 2012.

[4] M. Y. Hong, Y. H. Chang, A. Dienes, J. P. Heritage, and P. J. Delfyett, "Sub-picosecond pulse amplification in semiconductor laser amplifiers: Theory and experiment," IEEE J. Quantum Electron., vol. 30, pp. 1122–1131, 1994.

[5] M. J. Connelly, L. P. Barry, B. F. Kennedy, D. A. Reid, "Numerical analysis of picoseconds pulse propagation in a tensile-strained semiconductor optical amplifier with parameter extraction using frequency resolved optical gating", Optical and quantum electronics, vol. 40, Issue. 5-6, pp. 411-418, April 2008.

[6] N. K. Das, Y. Yamayoshi, and H. Kawaguchi, "Analysis of basic four wave mixing characteristics in a semiconductor optical amplifier by the finite-difference beam propagation method," IEEE Journal of Quantum Electronics, vol. 36, No. 10, pp. 1184–1192, October 2000.

[7] N. K. Das and N. C. Karmakar, "Nonlinear propagation and wave mixing characteristics of pulses in Semiconductor optical amplifiers," Microwave and Optical Tech. letters, vol. 50, No. 5, pp. 1223-1227, May 2008.

[8] S. R. Hosseini, M. Razaghi, and N. K. Das, "Analysis of ultrafast nonlinear phenomena's influences on output optical pulses and four-wave mixing characteristics in semiconductor optical amplifiers," Opt. Quantum Electron, vol. 42(11–13), pp. 729–737, April 2011.

[9] S. R. Hosseini, M. Razaghi, and N. K. Das, "Analysis of non-linear refractive index influences on four-wave mixing conversion efficiency in semiconductor optical amplifiers," Opt. Laser Tech., vol. 44(3), pp. 528–533, April 2012.

[10] M. Razaghi, A. Ahmadi, and M. J. Connelly, "Comprehensive finite-difference time-dependent beam propagation model of counter propagating picosecond pulses in a semiconductor optical amplifier," IEEE/OSA Journal of Lightwave Tech., vol. 27, No. 15, pp. 3162-3174, August 2009.

[11] N. K. Das, M. Razaghi, S. R. Hosseini, "Four-wave mixing in semiconductor optical amplifiers for high speed communication", 5th International conference on Computers and Devices for Communication (CODEC), pp. 1-4, December 2012.